Available online at www.sciencedirect.com
SCIENCE DIRECT
Thermochimica Acta 438 (2005) 102–106
thermochimica acta
www.elsevier.com/locate/tca

Non-isothermal kinetics studies on the thermal decomposition of zinc hydroxide carbonate

Zhongjun Li [a,*], Xiaoqing Shen [a], Xun Feng [b], Peiyuan Wang [a], Zhishen Wu [c]

[a] *Department of Chemistry, Zhengzhou University, Zhengzhou 450052, China*
[b] *Department of Chemistry, Luoyang Normal College, Luoyang 470122, China*
[c] *Laboratory of Special Functional Materials, Henan University, Kaifeng 475001, China*

Received 31 January 2005; received in revised form 18 August 2005; accepted 23 August 2005
Available online 30 September 2005

Abstract

Zinc hydroxide carbonate precursor, $Zn_4CO_3(OH)_6{\cdot}H_2O$, was synthesized from zinc sulfate using ammonium carbonate as a precipitating agent. Thermogravimetry (TG), differential scanning calorimetry (DSC), transmission electronic microscopy (TEM), infrared spectrum (IR) and X-ray diffraction (XRD) were used to characterize the precursor and the decomposed product. Non-isothermal kinetics of the thermal decomposition of zinc hydroxide carbonate were studied in nitrogen. Based on which, the kinetic parameters were obtained through mode-free method and the thermal decomposition mechanism was derived by mains of non-linear regression. The results show that the decomposition of zinc hydroxide carbonate acts as a double-step reaction, $A \overset{D2}{\longleftrightarrow} B \overset{Fn}{\longrightarrow} C$: a reversible reaction of two-dimensional diffusion (D2), with $E1 = 202\,kJ\,mol^{-1}$, $\lg(A1/s^{-1}) = 22.1$, is followed by an irreversible one of nth-order reaction (Fn) with $n = 0.51$, $E2 = 129\,kJ\,mol^{-1}$, $\lg(A2/s^{-1}) = 10.5$, and the decomposition of $Zn_4CO_3(OH)_6{\cdot}H_2O$ to ZnO is accompanied by the change in particle morphology and particle size.

Keywords: Thermal decomposition; Non-isothermal kinetics; Zinc hydroxide carbonate

1. Introduction

Zinc oxide (ZnO) is a technologically important material with a variety of applications such as solar cells, gas sensors, optoelectronic devices, varistors, and catalysts. Various techniques have been developed for the preparation of ZnO powders, which include liquid phase precipitation [1,2], sol–gel process [3,4], spray pyrolysis [5,6], and emulsion reaction [7,8]. Among these methods, the synthesis of ZnO powders via liquid phase precipitation of the precursor of zinc hydroxide carbonate and followed by thermal decomposition has received a considerable amount of attention, because the microstructural and physical properties of ZnO powders obtained can be modified and controlled by varying the precipitating process parameters and calcining conditions of the precursors [9–11].

The thermal decomposition of zinc hydroxide carbonate is an essential step for preparation of ZnO powders from the precipitated precursors. Investigation into the mechanism and kinetics of the thermal decomposition of zinc hydroxide carbonate can provide valuable information about the behavior of its thermal decomposition, which is also one of the important aspects that must be considered in the study of zinc oxide preparation.

Up to now, different forms of zinc hydroxide carbonate including $Zn_3CO_3(OH)_4{\cdot}2H_2O$, $Zn_5(CO_3)_2(OH)_6$ and $Zn_4CO_3(OH)_6{\cdot}H_2O$ have been used as the precursor to fabricate ZnO powders [9,12,13], and the decomposition kinetics of zinc hydroxide carbonates have been reported in the literatures [12–14]. However, there are disparities existed in thermal decomposition model and kinetics parameters among the zinc hydroxide carbonates obtained from different origins or prepared at different synthesis conditions. In the present work, zinc hydroxide carbonate precursor, $Zn_4CO_3(OH)_6{\cdot}H_2O$, was synthesized from zinc sulfate solution using ammonium carbonate as a precipitating agent and subsequently thermally treated. Thermogravimetry (TG), differential scanning calorimetry (DSC), transmission electronic microscopy (TEM), infrared spectrum (IR) and X-ray diffraction (XRD) were used to characterize the precursor and the obtained ZnO powders.

* Corresponding author. Tel.: +86 3717767255; fax: +86 3717761744.
E-mail address: lizhongjun@zzu.edu.cn (Z. Li).

0040-6031/$ – see front matter © 2005 Elsevier B.V. All rights reserved.
doi:10.1016/j.tca.2005.08.026

Based on the results of thermal analysis, the kinetic parameters of $Zn_4CO_3(OH)_6$ thermal decomposition have been calculated by employing mode-free methods and the reaction models have been derived by means of non-linear regression.

2. Experimental

2.1. Preparation of precursor

Zinc sulfate heptahydrate ($ZnSO_4{\cdot}7H_2O$) and ammonium carbonate ($(NH_4)_2CO_3$) were used as starting materials, both of them were of analytic reagent grade and used as-received without further purification. Zinc hydroxide carbonate precursor was synthesized by adding dropwise a zinc sulfate solution ($1.0\,mol\,L^{-1}$) into a rapidly stirred ammonium carbonate solution ($2.0\,mol\,L^{-1}$) at $37 \pm 1\,^{\circ}C$ in a mole ratio of $(NH_4)_2CO_3$ to $ZnSO_4$ equal to 1.1. The as-prepared precursor powder was filtered, washed thoroughly with deionized water to eliminate SO_4^{2-} ions, and then dried at room temperature under vacuum.

The isothermal calcination of the as-prepared precursor powder was carried out with an air atmosphere using about 3 g of samples. The decomposed products obtained at 300, 500 and 700 °C for 1 h were subjected for XRD and TEM analyses.

2.2. Sample characterization

The crystalline phases in the as-prepared and calcined products were identified by XRD with a Rigaku D/MAX-IIIB diffractometer using Cu Kα radiation. The particle morphology and size of the as-prepared and calcined powders were observed by TEM using a Jeol JEM-2010 electron microscope. Specimens were prepared by evaporation of an ethanolic dispersion of the powders on grids coated with perforated carbon film. The IR spectrum of the as-prepared powder was recorded using a Nicolet Nexus 470 FTIR spectrometer.

2.3. Thermal analysis

Thermal behaviors were measured on NETZSCH TG209 and DSC 204 instruments (Germany) in nitrogen atmosphere with the flow rate of 20 and 70 mL min^{-1}, respectively. Al_2O_3 crucibles were used for TG measurement and an Al crucible for DSC to hold about 3–5 mg of the samples, respectively. The heating rate for thermal decomposition employed was 10 °C min^{-1}, and the rates for kinetic analysis were 2.5, 5, 10, 15 and 20 °C min^{-1}, respectively. In kinetics experiments the precursor was pretreated in pure nitrogen atmosphere at 100 °C for 1 h to remove hydration water completely, and the range of temperature studied was from 100 to 350 °C.

3. Results and discussion

3.1. Characterization of zinc hydroxide carbonate

Fig. 1 shows the XRD pattern of the as-prepared precursor powder. It can be seen that the precursor powder displays almost all the characteristic diffractions corresponding to $Zn_4CO_3(OH)_6{\cdot}H_2O$ [15]. Chemical analysis revealed that the content of Zn in the powder was 58.85%, which was in accordance with the theoretical value (59.23%) in $Zn_4CO_3(OH)_6{\cdot}H_2O$. The TG–DSC curves of the precursor powder given in Fig. 2 show two endothermic peaks up to 340 °C, with a total weight loss of 27.1%, this weight loss is close to the theoretical mass loss (26.3%) calculated for $Zn_4CO_3(OH)_6{\cdot}H_2O$.The smaller endothermic peak located at about 60 °C, with weight loss of 3.9%, was caused by the release of hydration water. The larger peak at 252 °C, with weight loss of 23.2%, was due to the decomposition of $Zn_4CO_3(OH)_6$ into ZnO and the release of CO_2 and H_2O. The calculated weight losses for these two thermal events are 4.1% and 22.2%, respectively, which agree with those revealed by the TG curve.

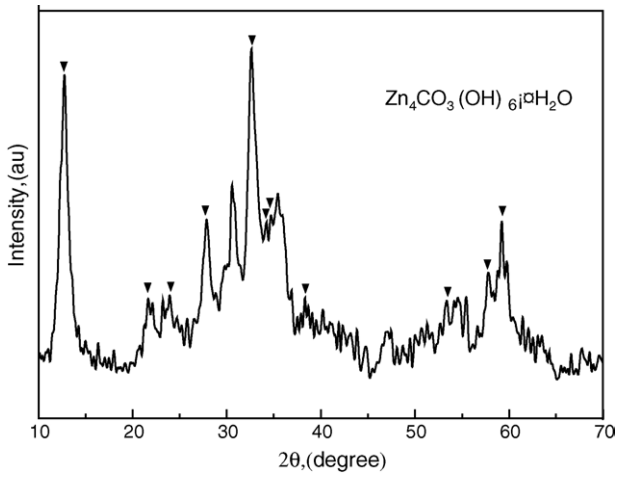

Fig. 1. XRD pattern of the as-prepared precursor powder.

The IR spectrum of the precursor powder is presented in Fig. 3. The band centered at 3364 cm^{-1} is the characteristic OH stretching vibration. The two strong bands at 1506 and 1385 cm^{-1} are attributed to υ_3 mode of carbonate, and the bands at 1046, 835 and 708 cm^{-1} are assigned to υ_1, υ_2 and υ_4 mode of carbonate, respectively [16]. The TEM micrograph of the precursor powder is given in Fig. 4, which shows that the precursor powder is composed of ellipsoidal $Zn_4CO_3(OH)_6{\cdot}H_2O$ particles, and the particle size is about 20–40 nm.

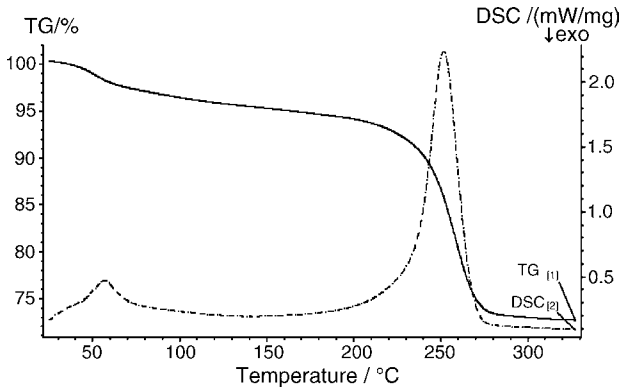

Fig. 2. TG–DSC curves of $Zn_4CO_3(OH)_6{\cdot}H_2O$.

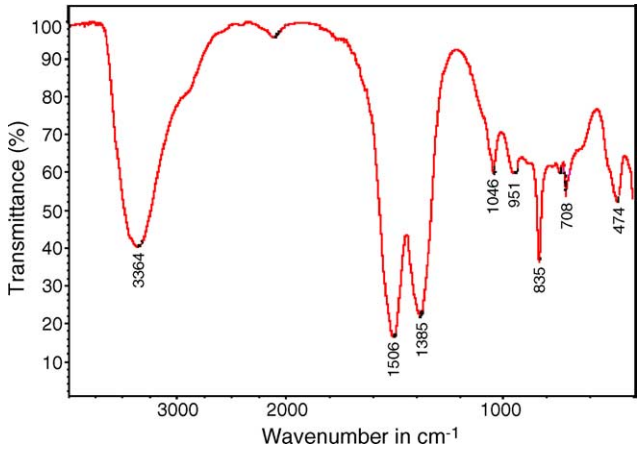

Fig. 3. IR spectrum of the precursor powder.

3.2. Non-isothermal kinetics of the thermal decomposition of $Zn_4CO_3(OH)_6$

3.2.1. Model-free estimation of activation energy

A series of dynamic scans with different heating rates results in a set of data, which exhibits the same degree of conversion (α) at different temperatures. Based on these, two methods of differential and integral are developed by Friedman as well as Ozawa–Flynn–Wall to determine the kinetic parameters without having to presuppose a certain model. Fig. 5 shows the TG curves of $Zn_4CO_3(OH)_6$ measured in N_2 atmosphere with the heating rate of 2.5, 5, 10,15 and 20 °C min^{-1}, respectively. The basic data (β, α, T) taken from the TG curves are used in the equations bellow:

Ozawa–Flynn–Wall equation [17,18]:

$$\ln \beta = \ln\left(\frac{AE}{R}\right) - \ln g(a) - 5.3305 - 1.052\frac{E}{RT} \quad (1)$$

where β is heating rate, α degree of conversion, $g(\alpha)$ mechanism function, E activation energy, A pre-exponential factor, and R gas constant.

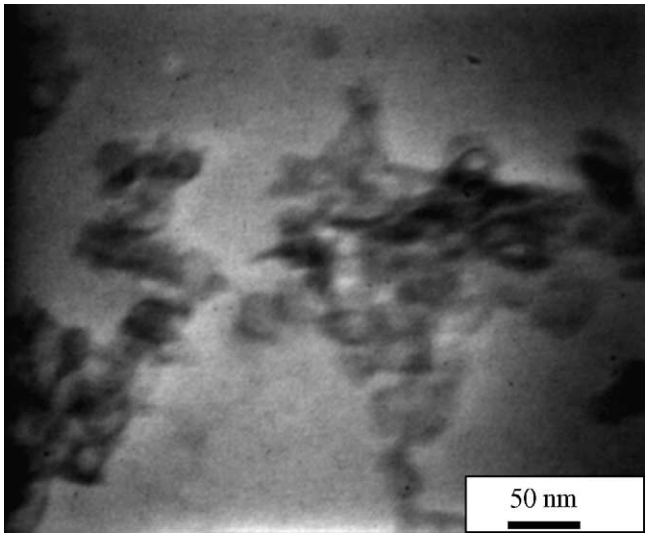

Fig. 4. TEM micrograph of the precursor powder.

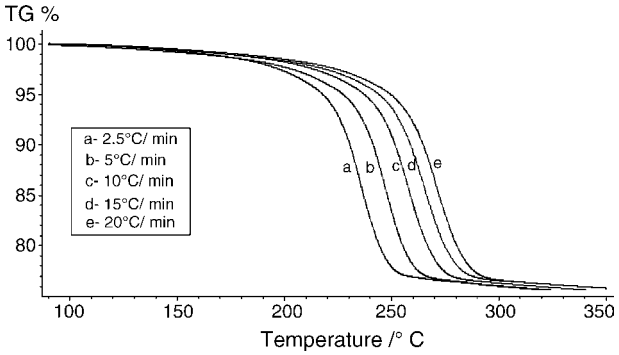

Fig. 5. TG curves with different heating rates. Heating rates listed are setting values.

Friedman equation [19]:

$$\ln\left(\frac{d\alpha}{dt}\right)_{\alpha=\alpha j} = \ln[Af(a)_j] - \frac{E}{RT} \quad (2)$$

where $d\alpha/dt$ is the rate of conversion, and $f(\alpha)$ mechanism function.

It can be seen from Eqs. (1) and (2) that the graphs $\ln \beta$ versus $1/T$ and $\ln(d\alpha/dt)$ versus $1/T$ both show straight lines with slopes $m_{(1)} = -1.052E/R$ and $m_{(2)} = -E/R$. The slopes of these straight lines are directly proportional to the reaction activation energy (E). Fig. 6 shows these lines at different α by means of OFW method and the calculated results using both Eqs. (1) and (2) are shown in Table 1.

From Table 1 it can be seen that the maximum values of E calculated using different methods are comparable, although the maximum of E appears at the different value of α. It is clear in Table 1, that the activation energy assumes a value of about 251 kJ mol^{-1} at the beginning of the decomposition reaction and, with increasing mass loss, drops to a average value of 124 kJ mol^{-1} (OFW method). This decreasing dependence of the activation energy on a indicates that the overall reaction contains at least two steps, and the kinetics scheme of which corresponds to a reversible reaction followed by an irreversible one [20–22], presumably, a main reaction with $E2$ at average value of 124.34 kJ mol^{-1}, is preceded by another

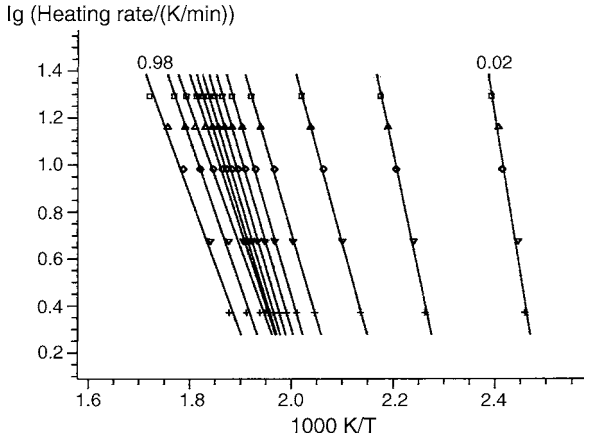

Fig. 6. OFW analysis of TG measurements on $Zn_4CO_3(OH)_6$ with β (°C min^{-1}): (+) 2.4, (▽) 4.8, (◇) 9.8, (△) 14.8 and (◯) 19.9.

Table 1
Parameters E (kJ mol^{-1}) and lg(A/s^{-1}) for the thermal decomposition of $Zn_4CO_3(OH)_6$

Degree of conversion (α)	Ozawa–Flynn–Wall analysis		Friedman analysis	
	E (kJ mol^{-1})	lg(A/s^{-1})	E (kJ mol^{-1})	lg(A/s^{-1})
0.02	251.63 ± 19.76	28.53	166.77 ± 81.19	16.83
0.05	189.14 ± 7.68	18.78	277.18 ± 31.35	28.34
0.10	143.72 ± 2.90	12.58	210.02 ± 12.35	19.51
0.20	133.71 ± 2.72	11.08	119.29 ± 9.62	9.52
0.30	132.06 ± 2.74	10.84	87.54 ± 5.17	6.25
0.40	131.60 ± 2.63	10.81	76.55 ± 3.33	5.17
0.50	131.35 ± 2.48	10.81	72.10 ± 2.58	4.76
0.60	130.23 ± 2.27	10.73	69.68 ± 2.45	4.58
0.70	126.34 ± 3.09	10.38	66.70 ± 3.26	4.39
0.80	117.19 ± 5.49	9.52	61.93 ± 5.28	4.07
0.90	106.13 ± 6.76	8.46	65.80 ± 7.93	4.66
0.95	111.68 ± 5.22	8.98	94.88 ± 11.57	7.60
0.98	103.68 ± 7.50	8.08	133.29 ± 26.91	11.28

reversible reaction as pre-reaction with $E1$ of 251 kJ mol^{-1} at $a < 0.1$. E is limited by the sum of the activation energy of the irreversible reaction and the enthalpy of the reversible reaction at low conversions, and by the activation energy of the irreversible reaction at high conversions [22]. Although the parameter data obtained above may contain some systematic errors, they would provide initial values for the non-linear regression (NLR) below to derive the reaction mode and would be optimized finally.

3.2.2. *Estimation of kinetic model by means of multiple linear regression (MLR)*

Non-linear regression [23] allows a direct fit of the model to the experimental data without a transformation and there are no limitations with respect to the complexity of the model. For this reason, NLR method can be used and iterative procedures can be employed for estimating of the reaction model of $Zn_4CO_3(OH)_6$.

Selecting mechanism function $f(\alpha)$ of different singular reaction types [24], testing two-step reaction types to which individual steps are linked as $A \overset{1}{\longleftrightarrow} B \overset{2}{\longrightarrow} C$, setting the initial values of the parameters of E and lg A according to OFW method, the calculation of the regress values is carried out by means of a 5th-degree RUNGE-KUTTA procedure using the Prince–Domand embedding formula for automatic optimization of the number of supporting digits [25]. To minimize the deviance, least squares (LSQ) method is used and a smooth convergence is ensured. All these work are performed under the procedure of NETZCH kinetic software.

The calculated curves were obtained by means of NLR. These curves were fitted to the experimental ones. During this procedure kinetic parameters of initial values are optimized to get high fitting quality. Considering fitting quality (characterized by correlation coefficient and relative precision), the kinetic scheme, $A \overset{D2}{\longleftrightarrow} B \overset{Fn}{\longrightarrow} C$, is the most suitable one for this reaction. The kinetic parameters and statistical characterization after the NLR are listed in Table 2 and graphic presentation of the curve fitting are shown in Fig. 7. It can be seen that the experimental data and the non-linear regression model fit well.

Table 2
Results of non-linear regression (NLR)

Kinetic parameters	Statistics
lg($A1$/s^{-1}): 22.0860	Correlation coefficient: 0.999341
$E1$ (kJ mol^{-1}): 201.60676	Rel. precision: 0.001000
lg($A2$/s^{-1}): 10.53467	Least squares: 197.10557
$E2$ (kJ mol^{-1}): 129.47800	Max. no. of cycles: 50
React. ord.: 0.50600	t-critical(0.95; 415): 1.955
Foll React. 1: 0.05380	Durbin–Watson factor: 3.65655

In short, the result of the kinetic analysis above shows that the decomposition of $Zn_4CO_3(OH)_6$ preferably performs as two-step reaction: a reversible reaction of two-dimensional diffusion (D2), with $E1 = 202$ kJ mol^{-1}, lg($A1$/s^{-1}) = 22.1, is followed by an irreversible one of nth-order reaction (Fn) with $n = 0.51$, $E2 = 129$ kJ mol^{-1}, lg($A2$/s^{-1}) = 10.5.

3.3. *Characterization of decomposed products*

In order to examine the phase structure as well as the particle size and morphology of the product of $Zn_4CO_3(OH)_6 \cdot H_2O$ ther-

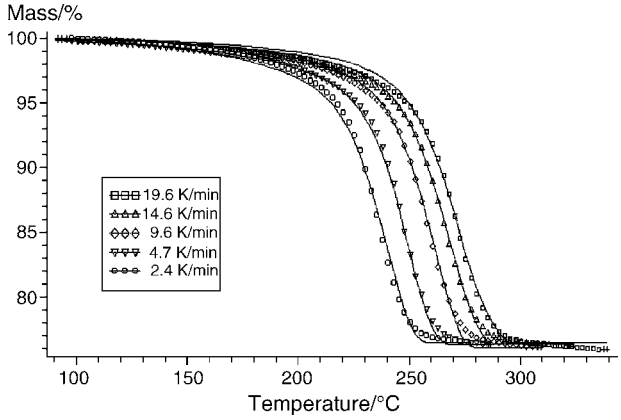

Fig. 7. Curve fitting for the decomposition of $Zn_4CO_3(OH)_6$, simulated with reaction types of D2 and Fn. (◯), (▽), (◊), (△), (□) experimental plots, (—) integral plots. Heating rates listed are measured values.

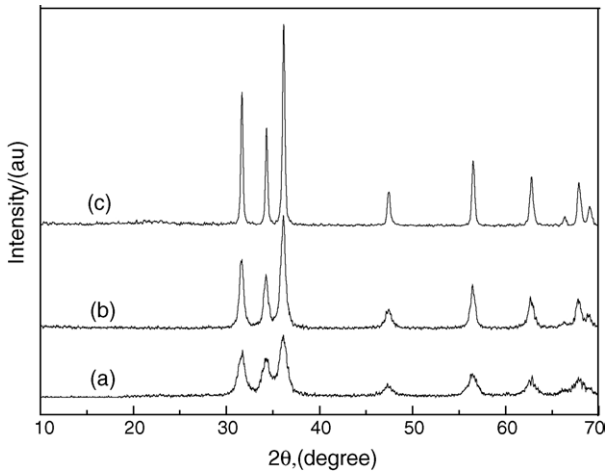

Fig. 8. XRD patterns of ZnO powders obtained at temperatures of 300 °C (a), 500 °C (b), and 700 °C (c).

mal decomposition, the powders obtained after isothermal calcinations were subjected to XRD and TEM analyses, the results of which are shown in Figs. 8 and 9, respectively. From Fig. 8 it can be seen that the powder calcined at 300 °C exhibits a diffraction pattern which matches the standard for hexagonal crystal ZnO [27] and no X-ray evidence can be found for the existence of other zinc carbonate phases in the powder. With increasing heating temperature from 300 to 700 °C, continued refinement in peak shapes and intensities is observed, this result indicates that although the decomposition of $Zn_4CO_3(OH)_6{\cdot}H_2O$ to ZnO has been accomplished at the temperature of 300 °C, increasing the calcination temperatures can make the crystalline growth of ZnO more perfect. The TEM analysis given in Fig. 9 shows

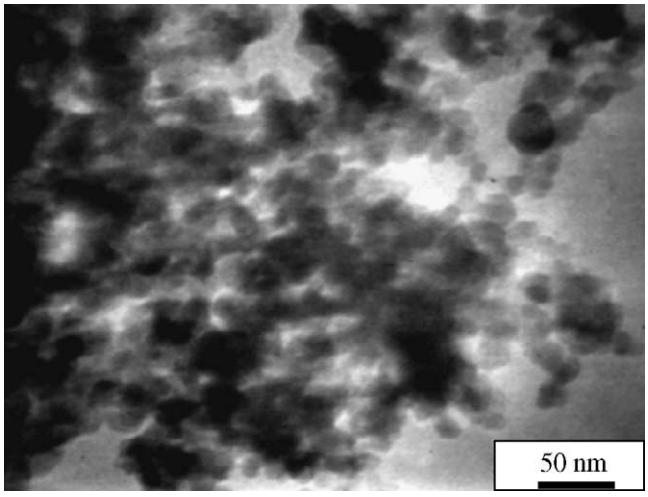

Fig. 9. TEM micrograph of the ZnO powder obtained at 500 °C.

that the ZnO powder obtained at 500 °C exhibits approximately spherical morphology, and the particle size is about 20–30 nm. Combining this result with that of Fig. 4 it can be seen that the decomposition of $Zn_4CO_3(OH)_6{\cdot}H_2O$ to ZnO is accompanied by the change in particle morphology and particle size.

Acknowledgements

This work was financially supported by the Innovation Fund for Outstanding Scholar of Henan Province (0521001100) and the Natural Science Foundation of Henan Province (0311020400).

References

[1] S.M. Haile, D.W. Johnson, J. Am. Ceram. Soc. 72 (1989) 2004.
[2] L.Q. Jing, Z.L. Xu, J. Shang, X.J. Sun, W.M. Cai, H.C. Guo, Mater. Sci. Eng. A 332 (2002) 356.
[3] R.J. Lanf, W.D. Bond, Am. Ceram. Soc. Bull. 63 (1984) 278.
[4] X.Y. Kang, T.D. Wang, Y. Han, M.D. Tao, Mater. Res. Bull. 32 (1997) 1165.
[5] X.Y. Zhao, B.C. Zheng, C.Z. Li, H.C. Gu, Powder Technol. 100 (1998) 20.
[6] Y.H. Lin, Z.L. Tang, Z.T. Zhang, J. Am. Ceram. Soc. 83 (2000) 2869.
[7] C. Lu, Y. Ceh, Mater. Lett. 33 (1997) 129.
[8] B.P. Lim, J. Wang, S.C. Ng, C.H. Chew, L.M. Gan, Ceram. Int. 24 (1998) 205.
[9] F.A. Sigoli, M.R. Davolos, M. Jafelicci Jr., J. Alloys Compd. 262–263 (1997) 292.
[10] S. Music, D. Dragcevic, M. Maljkovic, S. Popovic, Mater. Chem. Phys. 77 (2002) 521.
[11] L.Q. Jing, Z.L. Xu, X.J. Sun, J. Shang, W.M. Cai, Appl. Surf. Sci. 180 (2001) 308.
[12] Y.H. Liu, J.Z. Zhao, H. Zhang, Y.C. Zhu, Z.C. Wang, Thermochim. Acta 414 (2004) 121.
[13] J. Chen, R. Zhao, H. Jiang, Y. Li, G. Bao, Trans. Nonferrous Met. Soc. (China) 8 (1998) 149.
[14] N. Kanari, D. Mishra, I. Gaballah, B. Dupr, Thermochim. Acta 410 (2004) 93.
[15] Joint Committee on Powder Diffraction Standards (JCPDS), International Center for Diffraction Data (Files 11-0287), Swathmore, PA.
[16] S. Music, S. Popovic, M. Maljkovic, D. Dragcevic, J. Alloys Compd. 347 (2002) 324.
[17] T. Ozawa, Bull. Chem. Soc. Japan 38 (1965) 1881.
[18] J.H. Flynn, L.H. Wall, Polym. Lett. 4 (1966) 323.
[19] H.L. Friedman, J. Macromol. Sci. (Chem.) 41 (1967) 51.
[20] S. Vyazovkin, Int. Rev. Phys. Chem. 19 (1) (2000) 45.
[21] S. Vyazovkin, W. Linert, Int. J. Chem. Kinet. 27 (1995) 73.
[22] S. Vyazovkin, Int. J. Chem. Kinet. 28 (1996) 95.
[23] P.D.M. Benoit, R.G. Ferillo, A.H. Ganzow, Anal. Chim. Acta 124 (1985) 869.
[24] C.H. Bamford, C.F. Tipper (Eds.), Comprehensive Chemical Kinetics, Reactions in Solid State, vol. 22, Amsterdam 1980, pp. 57, 63.
[25] G. NETZSCH-Geratebau, Thermo-Kinetic Analysis: Multiple Scan, third ed., pp. 2–44.
[27] Joint Committee on Powder Diffraction Standards (JCPDS), International Center for Diffraction Data (Files 5-0664), Swathmore, PA.